JOURNAL OF THERMOPHYSICS AND HEAT TRANSFER
Vol. 9, No. 2, April–June 1995

Hypersonic Hydrogen Combustion in the Thin Viscous Shock Layer

Vladimir V. Riabov*
Worcester Polytechnic Institute, Worcester, Massachusetts 01609-2280
and
Andrei V. Botin†
Central Aerohydrodynamics Institute, Zhukovsky-3, Moscow Region 140160, Russia

Different models of hypersonic diffusive hydrogen combustion in a thin viscous shock layer (TVSL) at moderate Reynolds numbers have been developed. The study is based on computations of nonequilibrium multicomponent flowfield parameters of air-hydrogen mixture in the TVSL near the blunt probe. The structure of computed combustion zones is analyzed. Under conditions of slot and uniform injections the zone structures are essentially different. Hydrogen injection conditions are discovered at which the nonreacting hydrogen zone and the zone enriched with the hydrogen combustion products appear near the body surface. Hydrogen, water, and OH concentrations identify these zones. More effective cooling of the probe surface occurs at moderate injections compared to strong ones. Under the blowing conditions at moderate Reynolds numbers the most effective cooling of the body surface occurs at moderate uniform hydrogen injection. The results can be helpful for predicting the degree of supersonic hydrogen combustion in hypersonic vehicle engines.

Nomenclature

C_i = ρ_i/ρ, mass concentration of species i
D = shock wave location
G = $(\rho U)_{H2}/(\rho V)_\infty$, dimensionless mass flow of injected gas
G_0 = injection parameter G at a critical cylinder line
$g_{\alpha\beta}$ = metric tensor
h'_i = $2h_i/V_\infty^2$, dimensionless specific enthalpy of species i
h_i^0 = latent heat of species i, Eq. (6)
I_i = diffusion flux of species i
I_k^* = diffusion flux of k element
I'_q = $2I_q/(\rho_\infty V_\infty^3)$, dimensionless heat flux
L = characteristic dimension
M = molecular mass of mixture
M_i = molecular mass of species i
N = number of species
N^* = number of chemical elements
R = radius of blunt body nose
R_g = universal gas constant
Re_0 = $\rho_\infty V_\infty L/\mu(T_0)$, Reynolds number
Sm_{ij} = Schmidt numbers
T = temperature
T' = T/T_0, dimensionless temperature
T_0 = stagnation temperature
u^k = contravariant velocity vector components in curvilinear coordinate system
V_∞ = freestream velocity
x^k = dimension coordinates
α_w = slope coefficient
ε = Cheng' small perturbation parameter
μ = viscosity coefficient
ξ^k = x^k/L, k = 1, 2, and 3
ρ = density
ρ' = $\varepsilon\rho/\rho_\infty$, dimensionless density
φ = $C_{H2}/C_{H2,sto}$

Subscripts
i = species i
sto = stoichiometric parameter
w = wall conditions
0 = stagnation parameter
∞ = freestream parameter

Superscripts
α = first surface coordinate
β = second surface coordinate
$'$ = dimensionless parameter

Introduction

THE problem of supersonic combustion has been studied by many researchers (see the review of Billig[1]). Hydrogen combustion under the kinetic regime conditions at small Reynolds number $Re_0 < 100$ was analyzed.[2–6] The comparison[6] of the results indicated a strong correlation between experimental[5] and computational data,[2–4,6] obtained from different gasdynamic models. The main feature of the results received by means of the nonequilibrium multicomponent, thin viscous shock layer (TVSL) technique[6] is a monotonous decrease of the heat flux at the stagnation point, when the relative amount of hydrogen fuel G_0 increases from 0 to 0.12. The different types of heat flux distributions on the parabolic cylinder surface were studied by Botin and Riabov[6] in the cases of the slot and uniform hydrogen injections. The purpose of this study is to develop the model of the TVSL technique[7] at moderate Reynolds numbers $1500 > Re_0 > 100$, as well as the models of diffusive combustion of hydrogen, which is injected with different intensity from the surface of a blunt probe into airflow.

TVSL Approximation

The TVSL equations and boundary conditions were obtained by means of tensor analysis.[8] The summation convention as well as Greek indexes for surface coordinates were

Received March 30, 1994; presented as Paper 94-2027 at the AIAA/ASME 6th Joint Thermophysics and Heat Transfer Conference, Colorado Springs, CO, June 20–23, 1994; revision received Aug. 26, 1994; accepted for publication Oct. 14, 1994.

*Visiting Associate Professor, Department of Mechanical Engineering, 100 Institute Road. Member AIAA.
†Research Scientist, Rarefied Gas Dynamics Branch, Aerothermodynamics Division. Member AIAA.

used. The system of the TVSL equations was derived in the covariant form using physical variables.

In the fixed Cartesian coordinate system a parametric function of the body surface is presented as the following:

$$r = r_w(x^\alpha), \qquad \alpha = 1, 2$$

$$g_{\alpha\beta} = \frac{\partial r_w}{\partial x^\alpha} \cdot \frac{\partial r_w}{\partial x^\beta}, \qquad g = \det(|g^{\alpha\beta}|)$$

$$\Gamma^\gamma_{\alpha\beta} = \frac{1}{2} g^{\gamma\delta} \left(\frac{\partial g_{\alpha\delta}}{\partial x^\beta} + \frac{\partial g_{\beta\delta}}{\partial x^\alpha} - \frac{\partial g_{\alpha\beta}}{x^\delta} \right) \tag{1}$$

where $\Gamma^\gamma_{\alpha\beta}$ is the Christoffel symbol of the second kind.

The parameterization of the Euclidean space is carried out in the vicinity of the body surface as the following:

$$r = r_w(x^\alpha) + x^3 \boldsymbol{n}_w(x^\alpha)$$

$$\boldsymbol{n}_w = \left(\frac{\partial r_w}{\partial x^1} \times \frac{\partial r_w}{\partial x^2} \right) \Big/ \left(\left| \frac{\partial r_w}{\partial x^1} \times \frac{\partial r^w}{\partial x^2} \right| \right) \tag{2}$$

where $\boldsymbol{n}_w$ is the unit vector of the external normal. The curvilinear coordinate system x^α, x^3 was used in obtaining the TVSL equations.

Dimensionless variables are introduced:

$$\xi'^\alpha = \frac{x^\alpha}{L}, \quad \xi'^3 = \frac{x^3}{\varepsilon L}, \quad g'_{\alpha\beta} = g_{\alpha\beta}, \quad g' = g, \quad \Gamma'^\delta_{\alpha\beta} = \Gamma^\delta_{\alpha\beta} \cdot L$$

$$\Gamma'^3_{\alpha\beta} = \Gamma^3_{\alpha\beta} \cdot L, \quad u'^\alpha = \frac{u^\alpha}{V_\infty}, \quad u'^3 = \frac{u^3}{\varepsilon V_\infty}, \quad T' = \frac{T}{T_0}$$

$$H' = \frac{2H}{V_\infty^2}, \quad p' = \frac{p}{\rho_\infty V_\infty^2}, \quad \rho' = \frac{\varepsilon\rho}{\rho_\infty}, \quad C'_i = \frac{\rho_i}{\rho}, \quad h'_i = \frac{2h_i}{V_\infty^2}$$

$$W'_i = \frac{W_i \varepsilon L}{\rho_\infty V_\infty}, \quad I'_i = \frac{I_i}{\rho_\infty V_\infty^2}, \quad I'_q = \frac{2I_q}{\rho_\infty V_\infty^3}, \quad \mu' = \frac{\mu}{\mu_0}$$

$$\lambda' = \frac{\lambda}{\mu_0 C_{p\infty}}, \quad Sm_{ij} = \frac{\mu}{\rho D_{ij}}, \quad Re_0 = \frac{\rho_\infty V_\infty L}{\mu_0}$$

$$m' = \frac{1}{\varepsilon Re_0} \qquad i, j = 1, \ldots, N \tag{3}$$

where L is characteristic dimension ($L = R$); u^α is the contravariant component of the velocity vector in curvilinear coordinate system at the body surface; H is enthalpy, p is pressure, and ε is a small parameter used in the Cheng approximation[7] theory of a thin viscous shock layer.

The range of the variations of the coordinate ξ^3 was transformed to the unit range by means of normalization $\eta = \xi^3/D$, where D is the value of ξ^3, which is the location of the shock wave. Then the TVSL equations are as follows [index (′) is omitted]:

$$\frac{\partial(g^{1/2}\rho u^\alpha)}{\partial\xi^\alpha} + \frac{g^{1/2}}{D}\left[\frac{\partial(\rho u^3)}{\partial\eta} - \eta \frac{\partial D}{\partial\xi^\alpha} \frac{\partial(\rho u^\alpha)}{\partial\eta} \right] = 0$$

$$u^\beta \frac{\partial u^\alpha}{\partial\xi^\beta} + \frac{1}{D}\left(u^3 - \eta u^\beta \frac{\partial D}{\partial\xi^\beta} \right) \frac{\partial u^\alpha}{\partial\eta} + \Gamma^\alpha_{\beta\gamma} u^\beta u^\gamma$$

$$= -\frac{\varepsilon g_{\alpha\beta}}{\rho}\left(\frac{\partial p}{\partial\xi^\beta} - \frac{\eta}{D}\frac{\partial p}{\partial\eta}\frac{\partial D}{\partial\xi^\beta} \right) + \frac{1}{m\rho D^2}\frac{\partial}{\partial\eta}\left(\mu \frac{\partial u^\alpha}{\partial\eta} \right)$$

$$\frac{\partial p}{\partial\eta} = -\rho D \Gamma^3_{\alpha\beta} u^\alpha u^\beta$$

$$u^\alpha \frac{\partial H}{\partial\xi^\alpha} + \frac{1}{D}\left(u^3 - \eta u^\alpha \frac{\partial D}{\partial\xi^\alpha} \right) \frac{\partial H}{\partial\eta} = -\frac{1}{\rho D}\frac{\partial I_q}{\partial\eta}$$

$$u^\alpha \frac{\partial C_i}{\partial\xi^\alpha} + \frac{1}{D}\left(u^3 - \eta u^\alpha \frac{\partial D}{\partial\xi^\alpha} \right) \frac{\partial C_i}{\partial\eta} = \frac{W_i}{\rho} - \frac{1}{\rho D}\frac{\partial I_i}{\partial\eta}$$

$$1 \le i \le N - N^*$$

$$u^\alpha \frac{\partial C^*_k}{\xi^\alpha} + \frac{1}{D}\left(u^3 - \eta u^\alpha \frac{\partial D}{\partial\xi^\alpha} \right) \frac{\partial C^*_k}{\partial\eta} = -\frac{1}{\rho D}\frac{\partial I^*_k}{\partial\eta}$$

$$1 \le k \le N^* - 1$$

$$\sum_{i=1}^{N} C_i = 1, \quad \sum_{i=1}^{N} I_i = 0 \tag{4}$$

The total enthalpy was calculated by this formula:

$$H = \sum_{i=1}^{N} C_i h_i + \frac{1}{2} g_{\alpha\beta} u^\alpha u^\beta \tag{5}$$

Specific enthalpy h_i was determined by means of the concept[9] of the Gibbs thermodynamic potential and the approximation formula:

$$h_i(T) = h_i^0 + \sum_{j=1}^{4} a_{ij} (10^{-4} T)^j \tag{6}$$

The polynomial coefficients a_{ij} are given in Ref. 9.

The heat capacity was determined as the following:

$$C_p = \sum_{j=1}^{N} C_{pj} C_j, \qquad C_{pj} = \frac{\mathrm{d}h_j}{\mathrm{d}T} \tag{7}$$

The expressions for diffusion flux (or Stefan–Maxwell equations[10]), pressure, and heat flux should be added to Eqs. (4) as the following:

$$\frac{m\mu}{D}\frac{\partial C_i}{\partial\eta} = \frac{m\mu C_i}{D}\frac{\partial \sqrt{p}}{\partial\eta}\left(\frac{M_i}{M} - \sum_{j=1}^{N}\frac{C_j M_j}{M} \right) + \sum_{j=1}^{N} Sm_{ij}\frac{M}{M_j}$$

$$\times (I_j C_i - I_i C_j) - C_i \sum_{j=1}^{N}\sum_{k=1}^{N} Sm_{kj}\frac{M}{M_j}(I_j C_k - I_k C_j)$$

$$i = 1, \ldots, N-1, \qquad p = \frac{\rho R_\infty T}{M}$$

$$I_q = -\frac{m}{D}\left[\lambda\frac{\partial T}{\partial\eta} + \mu\frac{\partial(g_{\alpha\beta}u^\alpha u^\beta)}{\partial\eta} \right] + \sum_{i=1}^{N} h_i I_i \tag{8}$$

The transfer coefficients of multicomponent nonequilibrium mixture were calculated using the approximation formulas[11,12] developed by Wilke[20] and Mason and Saxena.[21] The parameters of intermolecular potential energy and the collision integrals were calculated by the method of Riabov.[12] According to this method the exponential approximation of the additive potential function for atom-molecule and molecule-molecule collisions were used. The application of the additive potential under high-temperature conditions provides a higher level of accuracy for the transfer property calculations compared to the Lennard–Jones potential computations.

The approximation method is based on a bifurcation of binary diffusion coefficients.[13] This hypothesis leads to essential reduction of the amount of calculations that are necessary for the transfer coefficient computations, and it also provides admissible accuracy of the results.

External boundary conditions at $\eta = 1$ are the generalized Rankine–Hugoniot conditions[14]:

$$U^3_\infty - \rho\left(u^3 - u^\alpha \frac{\partial D}{\partial \xi^\alpha}\right) = 0$$

$$U^3_\infty(u^\beta - u^\beta_\infty) - \frac{m\mu}{D}\frac{\partial u^\beta}{\partial \eta} = 0$$

$$(U^3_\infty)^2 - p = 0, \qquad U^3_\infty = \frac{u^3_\infty}{V_\infty}$$

$$U^3_\infty(H - H_\infty) + I_q = 0$$

$$U^3_\infty(C_i - C_{i\infty}) + I_i = 0, \qquad 1 \le i \le N - N^*$$

$$U^3_\infty(C^*_k - C^*_{k\infty}) + I^*_k = 0, \qquad 1 \le k \le N^* - 1 \quad (9)$$

The first boundary condition of Eq. (9) is used for defining unknown shock wave location $D(\xi^\alpha)$.

Boundary conditions at the body surface are

$$u^\alpha = 0, \qquad T = T_w$$

$$\rho u^3 = G, \qquad G = (\rho U)_w/(\rho V)_\infty$$

$$I_i + k_{wi}\rho C_i + \rho u^3 C_i = 0, \qquad i = 1, \ldots, N - N^*$$

$$I^*_k + k_{wk}\rho C^*_k + \rho u^3 C^*_k = 0, \qquad k = 1, \ldots, N^* - 1 \quad (10)$$

where k_{wi} are the catalytic coefficients.

Mathematical description of the nonequilibrium process of hydrogen combustion considered 11 gas components of three elements: O_2, N_2, NO, H_2O_2, HO_2, H_2O, OH, H_2, H, O, N. It is suggested that 35 nonequilibrium homogeneous chemical reactions take place under the conditions of extreme mechanism of hydrogen combustion. The data on constants of forward and backward reaction rates are in the review of Dimitrov.[15] The constants of the reaction rates W_i of the limit mechanism of the air-hydrogen combustion were used in the calculations.[15] This mechanism is maximal in terms of combinatorics, i.e., any selection of reactions out of the reaction system is also a partial mechanism that approximates a particular chemical process under certain physical conditions, but with less accuracy.

The solution of one-dimensional equations at the stagnation streamline was used as the initial conditions of the marching computational procedure for the parabolized equation system Eqs. (4). These equations were obtained as the limit $u_1 \to 0$ applied to the system of Eqs. (4) and boundary conditions [Eqs. (9) and (10)]. The system of one-dimensional equations follows:

$$D\rho U^1_1 + \frac{\partial(\rho u^3)}{\partial \eta} = 0$$

$$D\rho(U^1_1)^2 + \rho u^3 \frac{\partial U^1_1}{\partial \eta} = -\frac{\varepsilon D P_{11}}{g_{11}} + \frac{1}{mD}\frac{\partial}{\partial \eta}\left(\mu \frac{\partial U^1_1}{\partial \eta}\right)$$

$$\rho u^3 \frac{\partial u^2}{\partial \eta} = \frac{1}{mD}\frac{\partial}{\partial \eta}\left(\mu \frac{\partial u^2}{\partial \eta}\right)$$

$$\frac{\partial p}{\partial \eta} = 0, \qquad \frac{\partial P_{11}}{\partial \eta} = -D\rho g^3_{11}(U^1_1)^2$$

$$\rho u^3 \frac{\partial H}{\partial \eta} = -\frac{\partial I_q}{\partial \eta}$$

$$\rho u^3 \frac{\partial C_i}{\partial \eta} = DW_i - \frac{\partial I_i}{\partial \eta}, \qquad 1 \le i \le N$$

$$\rho u^3 \frac{\partial C^*_k}{\partial \eta} = -\frac{\partial I^*_k}{\partial \eta}, \qquad 1 \le k \le N^* \quad (11)$$

The boundary conditions at the body surface and shock wave are the results of the substitute of u_1 for U^1_1. The terms that contain $\partial D/\partial \xi^\alpha$ are omitted from Eqs. (4) with the purpose of regularization. Additional boundary condition for the function P_{11} at the shock wave is

$$\left(\frac{\partial U^3_\infty}{\partial \xi_1}\right)^2 - P_{11} = 0 \quad (12)$$

Numerical Methods

The system of the nonequilibrium multicomponent TVSL Eqs. (4–12) is one of the simplest well-grounded mathematical models of viscous hypersonic flows.[7] Because of the hyperbolic type of the equations, the marching numerical procedure could be applied to calculate the flowfield parameters in a multidimensional case. A finite difference approximation to the TVSL equations and boundary conditions was constructed in analogy to the method[14] using a matrix variant of Keller's two-point box-scheme.[16] The algorithm of matrix factorization and standardized software of Babikov and Egorov[17,18] was used.

This method is based on the universal design of the structuring of the application programs. It permits the exclusion of essential transformation of the algorithms and reduction of routine computational time. The general procedure of the solution technique consisted of two stages. First, the solution of the regularized TVSL equations at the stagnation streamline was obtained using the adaptive grid along the variable ξ^3. The adaptive grid was designed in the process of solution of the regularized equations. Then it was fixed and used in the second stage in the marching process of the solution of Eqs. (4–10).

Modified Newton-Raphson method[19] was used for the numerical solutions of the nonlinear grid equations. The vector of corrections for each iteration was determined by the solution of the linearized system. The vector regularization procedure was used for the solution of the linearized system of the equations, both for one-dimensional flow at the stagnation streamline and for two-dimensional flow at the spreading line. The mass continuity equation from Eqs. (9) at the shock wave was used to calculate an unknown shock wave location $D(\xi^\alpha)$, which was considered as an independent variable. The iteration procedure was finished when the conditions $|\Delta F|_\infty \le 10^{-5}$ were realized for the vector of function corrections ΔF in the maximum (uniform) norm $|.|_\infty$ of the maximum absolute values of gasdynamic functions.

The accuracy evaluation[6] of the received results with the help of the created software was based on the comparison of flow characteristics in the critical point area within the range of Reynolds numbers with the results of calculations and experiments conducted by Lewis et al.,[2] Pappas and Lee,[4] and Davy et al.[5] Grid convergence requirements have been established previously in Refs. 6, 17, and 18.

Calculation Results

Critical Streamline

Slot injection was modeled as a hydrogen jet from the surface of infinite cylinder with generatrix and blunt radius $R = 0.015$ m, and $V_\infty = 2933$ m/s, $Re_0 = 628$, $T_\infty = 230$ K. It was assumed that the injected gas had wall temperature $T_w = 600$ K at absolutely noncatalytic surface. All variants were calculated using the adaptive grid with 41 nodes across the viscous layer. Grid convergence requirements have been established for a similar case in Refs. 6, 17, and 18. The injection from the body surface was simulated in terms of the injection parameter $G = G_0 \exp(-\alpha_w/\xi_1)$, where G_0 is the value of the injection parameter at the critical cylinder line, α_w is a coefficient characterizing the slope of "peak" curve $G(\xi_1)$ at modeling slot injection, and ξ_1 is marching coordinate along

generatrix of the body surface. The value α_w is 30 in these calculations.

Under the conditions at $Re_0 > 100$, the diffusion regime of the chemical reactions is realized. The concentrations of reaction products are large, and the reactions significantly effect the structure of the TVSL. Particularly, the diffusion of the "hot" reaction products occurs from the reaction zone to the body surface. This phenomenon leads to the increase of heat flux values at the surface.

Figure 1 presents profiles of excess hydrogen coefficient $\varphi = C_{H2}/C_{H2,sto}$ at the critical streamline; C_{H2} is hydrogen concentration in the viscous shock layer, and $C_{H2,sto}$ is its stoichiometric value. The parameter φ is very convenient for the identification of excess ($\varphi > 1$) and deficient ($\varphi < 1$) hydrogen zones in the TVSL. At small injections, $G_0 = 0.003$ (empty squares), the amount of hydrogen ($\varphi < 1$) is not sufficient for the development of chemical processes. At a moderate level of injections $0.05 \geq G_0 \geq 0.02$, there is a wide excess hydrogen zone at $\eta \leq 0.1$.

Profiles of the other species O_2, H_2O, and OH are shown in Figs. 2a, 2b, and 2c, respectively. The distribution of molecular oxygen across the TVSL indicates the reacting zones characterized by different types of reactions (see Fig. 2a). In the vicinity of the body surface at $\eta < 0.1$, molecular hydrogen is the major component of the mixture. At $0.25 > \eta > 0.1$, water concentration reaches its maximum value. As it is shown in Fig. 2b, this value is independent of the parameter G_0 at moderate injections. In the third zone at $0.5 > \eta > 0.25$, the distribution of molecular oxygen correlates well with the water distribution, and the concentration of OH molecules has its maximum value. The amount of the other air-hydrogen-combustion products is insignificant across the TVSL under considered conditions. The maximum values of H_2O and OH-concentrations determine the zones of different partial mechanisms of chemical reactions.

Two-Dimensional Flow Analysis, Slot Injection

Computational modelling of slot injection, using exponential law $G(\xi^1)$, indicates the presence of nonreacting molecular hydrogen near the body in all computational regions. Hydrogen is present in the flowfield regardless of the rapidly decreasing parameter along the marching coordinate (see Figs. 3a, and 4). The mixture appears to have hydrogen ($\varphi > 1$) near the body surface at moderate and strong injections when $G_0 > 0.01$. On the other hand, the mixture has a significant deficiency of hydrogen ($\varphi < 1$) near the external boundary of the TVSL. The mixture is hydrogen deficient ($\varphi < 1$) in all calculated fields when the injection is weak at $G_0 \leq 0.003$ (see Fig. 4). The presence of a hydrogen sublayer is observed in the area near the wall.

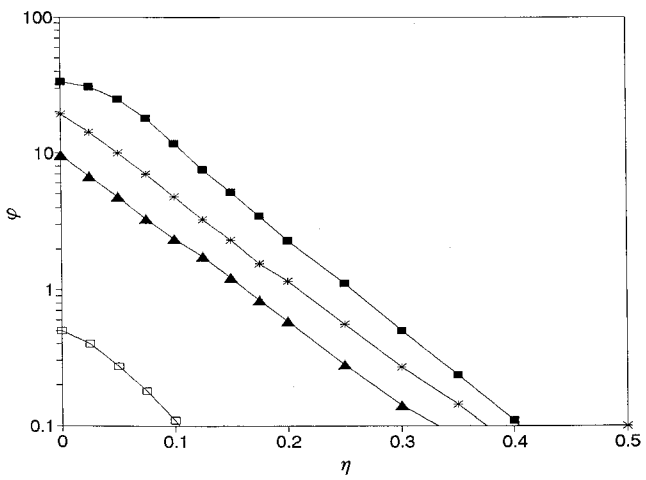

Fig. 1 Profiles of excess hydrogen coefficient φ: □, $G_0 = 0.003$; ▲, $G_0 = 0.02$; *, $G_0 = 0.03$; ■, $G_0 = 0.05$.

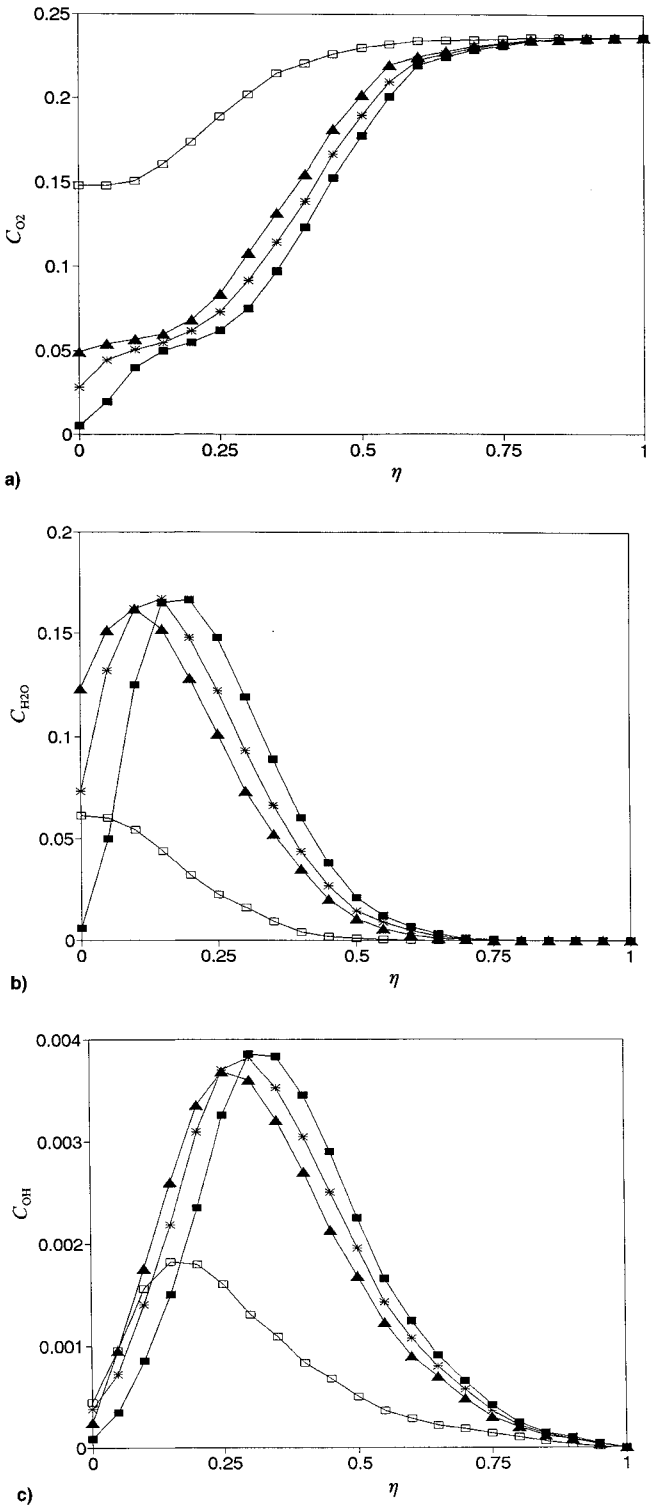

Fig. 2 Species mass concentration in the TVSL at the stagnation streamline: a) O_2, b) H_2O, and c) OH.

The combustion reactions producing water as the main final product occur in the field even if $G \to 0$. The profiles of C_{H2O} stabilize in one level at the distances that are far from the critical line or injection zone (see Fig. 3b). It is noted that the maximum of water concentration is in the TVSL region of excess hydrogen. On the other hand, the OH concentration has maximum value in the hydrogen deficient area (see Fig. 3c). The values of concentrations of the secondary reaction products (HO_2 and especially H_2O_2) are much less than the values of the remaining components in the TVSL, and that is why they are not considered in detail.

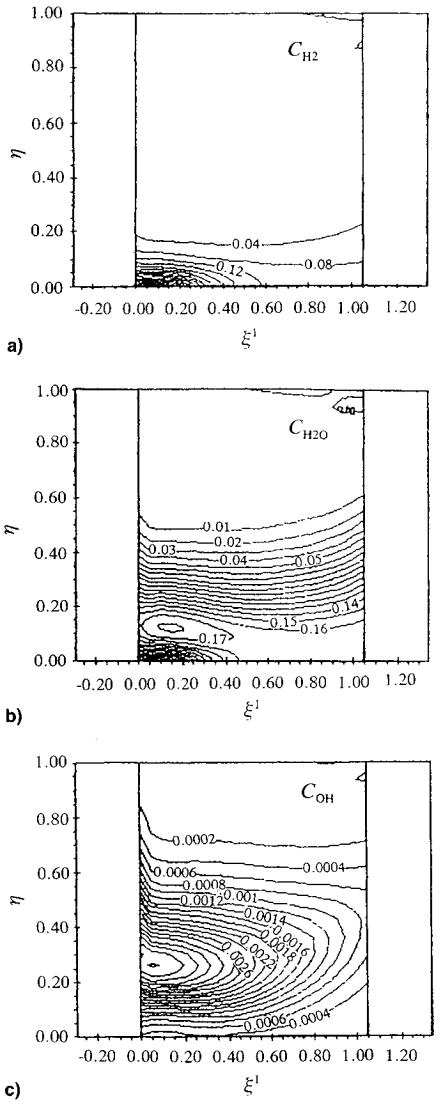

Fig. 3 Mass concentration of species at slot injection parameter $G_0 = 0.03$: a) H_2, b) H_2O, and c) OH.

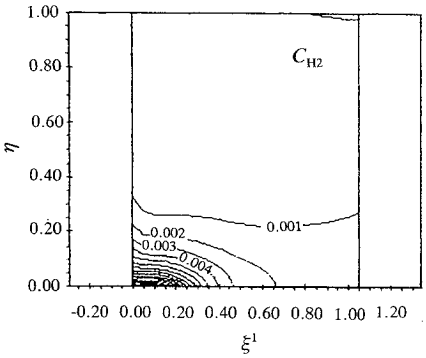

Fig. 4 Mass concentration of molecular hydrogen at small slot injection parameter $G_0 = 0.003$.

Figure 5 presents distributions of the normalized values of the heat flux I'_q towards the body surface along the coordinate ξ^1.

The heat from combustion reactions does not prevail over the cooling effect of injection at the considered Reynolds number, regardless of the presence of the combustion zone in the viscous shock layer. Even at a low level of injection near the injection zone, the local heat flux toward the body

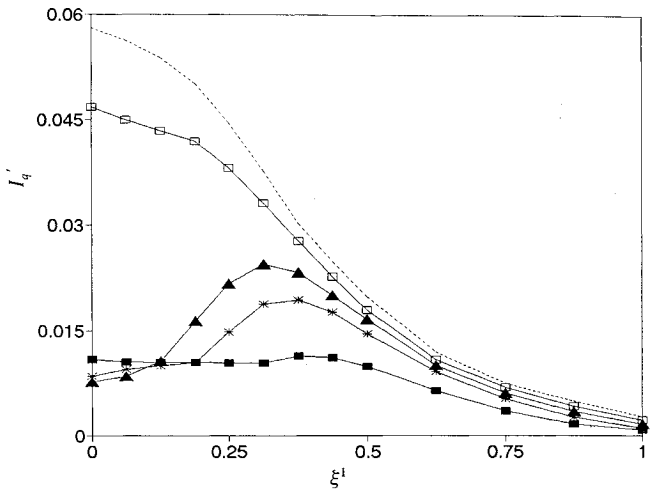

Fig. 5 Heat flux on parabolic cylinder at slot injection: dashed line, $G_0 = 0$; □, $G_0 = 0.003$; ▲, $G_0 = 0.02$; *, $G_0 = 0.03$; ■, $G_0 = 0.05$.

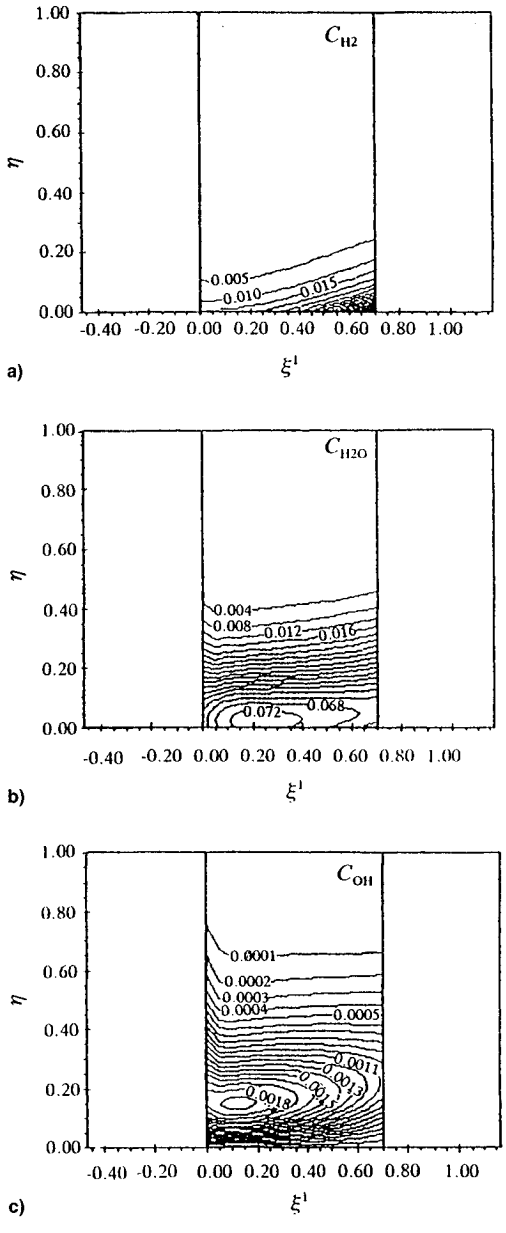

Fig. 6 Mass concentration of species at uniform injection parameter $G_0 = 0.003$: a) H_2, b) H_2O, and c) OH.

surface significantly decreases (see empty squares in Fig. 5). The heat flux is significantly lower than I'_q at $G_0 = 0$ near the injection zone at moderate injections ($0.02 \leq G_0 \leq 0.05$). But at the increase of the marching coordinate it begins to increase, and at $\xi^1 > 0.3$ the heat flux value practically does not differ from its value when the injection does not occur. A large quantity of injected hydrogen leads to effective cooling of the surface at a large distance from the injection zone at a high level of injection (see filled squares in Fig. 5). The zone of combustion moves from the surface of the body towards the external boundary of the TVSL as the injection intensity increases (see Fig. 3).

Two-Dimensional Flow Analysis, Uniform Injection

Cooling the porous surface of the infinite parabolic cylinder was modeled with the help of the intensity of hydrogen injection that was constant along the coordinate ξ^1, i.e., $G = G_0 = \text{const}$. The values of the upstream flow parameters were the same as mentioned above. Contrary to the above case of slot injection, the hydrogen fraction monotonously increases in the sublayer near the wall moving along the marching coordinate for small amounts of uniformly injected hydrogen, i.e., $G_0 = 0.003$ (see Fig. 6a). The hydrogen fraction reaches its maximum value at the surface at $\xi^1 \sim 0.65$. Water fraction

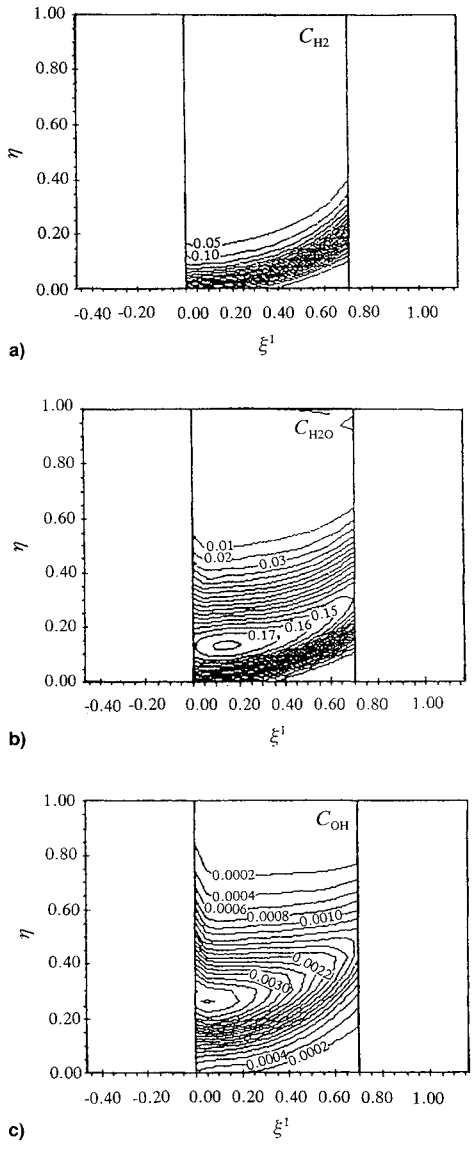

Fig. 7 Mass concentration of species at uniform injection parameter $G_0 = 0.03$: a) H_2, b) H_2O, and c) OH.

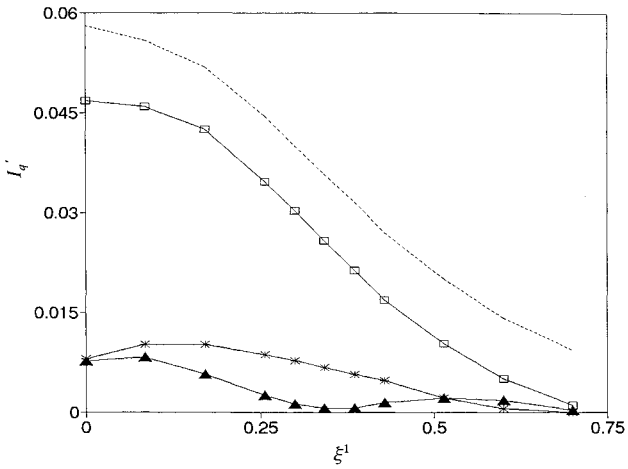

Fig. 8 Heat flux on parabolic cylinder at uniform injection: dashed line, $G_0 = 0$; □, $G_0 = 0.003$; ▲, $G_0 = 0.02$; *, $G_0 = 0.03$.

is significant in the region $0.6 > \xi^1 \geq 0$ near the wall. The maximum value of OH concentration is observed at some distance from the wall (see Figs. 6b and 6c).

At moderate ($G_0 = 0.02$) and strong ($G_0 \geq 0.03$) hydrogen injections the combustion zone ($\varphi \sim 1$) is far from the body surface. Figures 7a–7c show that its location approaches the external boundary of the TVSL when the marching coordinate increases. At $\xi^1 \sim 0.65$ the zone of maximum concentrations of H_2O, and OH is at the middle of the viscous layer.

This phenomenon is a result of displacing the flow by uniformly injected hydrogen at $G_0 \geq 0.02$.

The discovered flow features could be of great help for study of the local heat flux distributions at the cylinder surface in this case, which are shown in Fig. 8.

More significant decrease of the heat flux is found at the whole body surface, compared to the case of slot injection. At the weak injections (empty squares in Fig. 8) the heat flux at the entire computational region is less than I'_q in the absence of the injection, i.e., $G_0 = 0$.

The distribution of the heat flux toward the surface becomes noticeably distinct at moderate (triangles, $G_0 = 0.02$) and strong (asterisk, $G_0 = 0.03$) injections, as the result of mutual influence of thermophysical properties of hydrogen, high values of enthalpy of upstream flow, and the presence of combustion zone in the viscous shock layer.

Conclusions

The principal goal of this research was the development of a numerical tool in order to study the process of diffusive hydrogen combustion in a thin viscous shock layer at moderate Reynolds numbers. The algorithm is based on the use of a matrix factorization variant of Keller's two-point box-scheme combined with the modified Newton–Raphson method for the numerical solutions of the nonlinear grid equations. The numerical results indicate quite clearly under which conditions of slot and uniform injections the process of combustion is characterized by excess or deficient hydrogen zones. The major reaction products are water and OH, which could be effectively used for the identification of these zones.

At moderate Reynolds numbers the most effective cooling of the body surface occurs at moderate hydrogen injection and uniform distribution of the injection intensity along the marching coordinate.

References

[1]Billig, F. S., "Research on Supersonic Combustion," *Journal of Propulsion and Power*, Vol. 9, No. 4, 1993, pp. 499–514.

[2]Lewis, C. H., Adams, J. C., and Gilley, G. E., "Effects of Mass Transfer and Chemical Nonequilibrium on Slender Blunted Cone

Pressure and Heat Transfer Distributions at $M = 13.2$," Arnold Engineering and Development Center TR-68-214, 1968.

[3]Miner, E. W., and Lewis, C. H., "Hypersonic Ionizing Air Viscous Shock Layer Flows over Nonanalytic Blunt Bodies," NASA CR-2550, May 1975.

[4]Pappas, C. C., and Lee, G., "Heat Transfer and Pressure on a Hypersonic Blunt Cone with Mass Addition," *AIAA Journal*, Vol. 8, No. 8, 1970, pp. 984–995.

[5]Davy, W. C., Craig, R. A., and Lyle, G. C., "An Evaluation of Approximations Used in the Analysis of Chemically Reacting Stagnation Point Boundary Layers with Mass Injection," *Proceedings of the 1970 Heat Transfer and Fluid Mechanics Institute*, Stanford Univ. Press, Stanford, CA, 1970, pp. 222–237.

[6]Botin, A. V., and Riabov, V. V., "Injection of Hydrogen into the Thin Viscous Shock Layer," *Aerodynamics and Experimental Methods. Transactions of the 10th All-Union Conference on Rarefied Gas Dynamics*, Vol. 2, Moscow Energy Inst., Moscow, 1991, pp. 71–78 (in Russian).

[7]Cheng, H. K., "The Blunt-Body Problem in Hypersonic Flow at Low Reynolds Number," Cornell Aeronautical Lab., AF-1285-A-10, Buffalo, New York, 1963.

[8]McConnell, A. J., *Application of Tensor Analysis*, Dover, New York, 1957.

[9]Glushko, V. P., *Thermodynamic Properties of Individual Substances*, Nauka, Moscow, 1982 (in Russian).

[10]Tirsky, G. A., "Up-to-Date Gasdynamic Models of Hypersonic Aerodynamics and Heat Transfer with Real Gas Properties," *Annual Review of Fluid Mechanics*, Vol. 25, 1993, pp. 151–181.

[11]Lapin, Yu. V., *Turbulent Boundary Layer in Supersonic Gas Flow*, Nauka, Moscow, 1982 (in Russian).

[12]Riabov, V. V., "Transfer Coefficients of Multicomponent Air with Sublimation Products of Graphite," *Journal of Engineering Physics*, Vol. 55, No. 1, 1988, pp. 786–791.

[13]Bartlett, E. P., Kendall, R. M., and Rindal, R. A., "A Unified Approximation for Mixture Transport Properties for Multicomponent Boundary-Layer Applications," NASA CR-1063, June 1968.

[14]Provotorov, V. P., and Riabov, V. V., "Investigation of a Structure of a Multicomponent Viscous Shock Layer," *Trudy TsAGI*, Issue 2436, 1990, pp. 152–164 (in Russian).

[15]Dimitrov, V. P., *Simple Kinetics*, Nauka, Novosibirsk, Russia, 1982 (in Russian).

[16]Keller, H. B., "Accurate Difference Methods for Nonlinear Two-Point Boundary Value Problems," *SIAM Journal on Numerical Analysis*, Vol. 11, No. 2, 1974, pp. 305–320.

[17]Babikov, P. E., and Egorov, I. V., "On the Version of the Method of the Adaptive Grid Generation to Solve Evolution Problems," *Soviet Union—Japan Symposium on Computational Fluid Dynamics* (Khabarovsk, Russia), Nauka, Moscow, 1988, p. 15.

[18]Egorov, I. V., and Zaitsev, O. L., "An Approach to the Numerical Solution of the Two-Dimensional Navier-Stokes Equations by a Finite Difference Method," *Journal of Computational Mathematics and Mathematical Physics*, Vol. 31, No. 2, 1991, pp. 286–299.

[19]Anderson, A. D., Tannehill, C. J., and Pletcher, H. R., *Computational Fluid Mechanics and Heat Transfer*, Hemisphere, New York, 1984.

[20]Wilke, C. R., "A Viscosity Equation for Gas Mixtures," *Journal of Chemical Physics*, Vol. 18, No. 4, 1950, pp. 517–519.

[21]Mason, E. A., and Saxena, S. C., "Approximation Formula for the Thermal Conductivity of Gas Mixtures," *Physics of Fluids*, Vol. 1, No. 5, 1958, pp. 361–369.